Supplementary Materials

Nonvolatile Electrical Control of Spin Polarization in the 2D Bipolar Magnetic Semiconductor VSeF

Yuhui Li [1,2], Jun Deng [1,2], Yan-Fang Zhang [2], Xin Jin [2], Wen-Han Dong [1,2], Jia-Tao Sun [3], Jinbo Pan [1,2,4], Shixuan Du [1,2,4,5*]*

[1] Beijing National Laboratory for Condensed Matter Physics, Institute of Physics, Chinese Academy of Sciences, Beijing 100190, China

[2] University of Chinese Academy of Sciences, Chinese Academy of Sciences, Beijing 100190, China

[3] School of Integrated Circuits and Electronics, MIIT Key Laboratory for Low-Dimensional Quantum Structure and Devices, Beijing Institute of Technology, Beijing 100081, China

[4] Songshan Lake Materials Laboratory, Dongguan 523808, China

[5] CAS Center for Excellence in Topological Quantum Computation, Beijing 100190, China

* Corresponding authors. E-mail address: Pan, J. (jbpan@iphy.ac.cn), Du, S. (sxdu@iphy.ac.cn)

Supplementary Table 1. The calculated results of MXY compounds (M = Ti, V, Cr, Mn, Fe, Co, Ni, X = O, S, Se, Te, Y = F, Cl, Br, I) with dynamical stability. They are classified into four categories (nonmagnetic metals, nonmagnetic semiconductors, magnetic metals and magnetic semiconductors).

Nonmagnetic metals	TiSBr, TiSeF
Nonmagnetic semiconductors	CoSF, CoSCl, CoSBr, CoSI
Magnetic metals	TiTeF, VTeCl, VTeBr, VTeI, CrSeF, CrSeCl, CrTeF, CrTeCl, CrTeBr, CrTeI, MnTeBr, CoSeCl, CoSeBr, CoSeI, CoTeF, CoTeCl, CoTeBr, CoTeI, NiSCl, NiSBr, NiSI
Magnetic semiconductors	VSF, VSeF, VSeBr, CrSCl, CrSBr, CrSI, CrSeBr, CrSeI

Supplementary Table 2. The optimized lattice constant of VSeF monolayer (Å), exchange coupling constants J_1, J_2 and J_3 (meV), single-ion anisotropy A_x and A_y (μeV) and three energy gaps related to BMS feature Δ_1, Δ_2 and Δ_3 (eV) (PBE+U functional)

a	b	J_1	J_2	J_3	A_x	A_y	Δ_1	Δ_2	Δ_3
3.36	5.29	-3	12	-2	275	658	0.42	0.29	1.12

Supplementary Table 3. Relative energies (meV·f.u.$^{-1}$) of different magnetic configurations (Supplementary Fig. 3) for VSeF monolayer considering SOC effect.

E(FM)	E(AFM1)	E(AFM2)	E(AFM3)	E(AFM4)
0	48.9	18.7	14.6	20.8

Supplementary Table 4. Relative energies (meV) of different magnetic configurations (Supplementary Fig. 3) for pristine VSeF, VSeF/Al_2Se_3 bilayer heterostructure (upward and downward electric polarization) and VSeF/biAl_2Se_3 trilayer heterostructure (upward and downward electric polarization). E [010] and E [100] are magnetic anisotropic energies along y direction and x direction considering SOC effect, respectively, relative to the out-of-plane magnetic axis.

	E(FM)	E(AFM1)	E(AFM2)	E(AFM3)	E(AFM4)	E [010]	E [100]
Pristine VSeF	0	389	148	117	166	5	2
VSeF/Al_2Se_3 (↑)	0	384	166	124	151	5	2
VSeF/Al_2Se_3 (↓)	0	379	141	100	150	7	2
VSeF/biAl_2Se_3 (↑)	0	380	195	152	142	4	2
VSeF/biAl_2Se_3 (↓)	0	390	128	121	153	4	1

Supplementary Table 5. The structure difference of VSeF layer before and after structural relaxation in VSeF/Al_2Se_3 and VSeF/biAl_2Se_3 heterostructures. Here, the atomic labels are indicated in Supplementary Fig. 4. The units of distance between magnetic atoms (d) and angels among magnetic atoms and anion ligand (θ) are angstrom (Å) and degree (°), respectively. The values in brackets are the relative variations compared to pristine VSeF.

	d(V5-V7)	θ(V5-Se3-V7)	θ(V5-F7-V7)	d(V5-V3)	θ(V5-Se3-V3)	θ(V5-Se5-V6)
Pristine VSeF	3.36	81.3	112.3	3.83	93.8	169.9
VSeF/Al_2Se_3 (↑)	3.36 (0%)	81.4 (0.1%)	111.9 (-0.3%)	3.80 (-0.7%)	93.2 (-0.6%)	171.9 (1.2%)
VSeF/Al_2Se_3 (↓)	3.36 (0%)	81.2 (-0.1%)	113.0 (0.6%)	3.81 (-0.5%)	93.3 (-0.5%)	171.5 (0.9%)
VSeF/biAl_2Se_3 (↑)	3.36 (0%)	81.6 (0.3%)	110.6 (-1.5%)	3.80 (-0.7%)	93.2 (-0.6%)	172.2 (1.3%)
VSeF/biAl_2Se_3 (↓)	3.36 (0%)	80.9 (-0.5%)	114.0 (1.5%)	3.82 (-0.3%)	93.5 (-0.3%)	170.6 (0.4%)

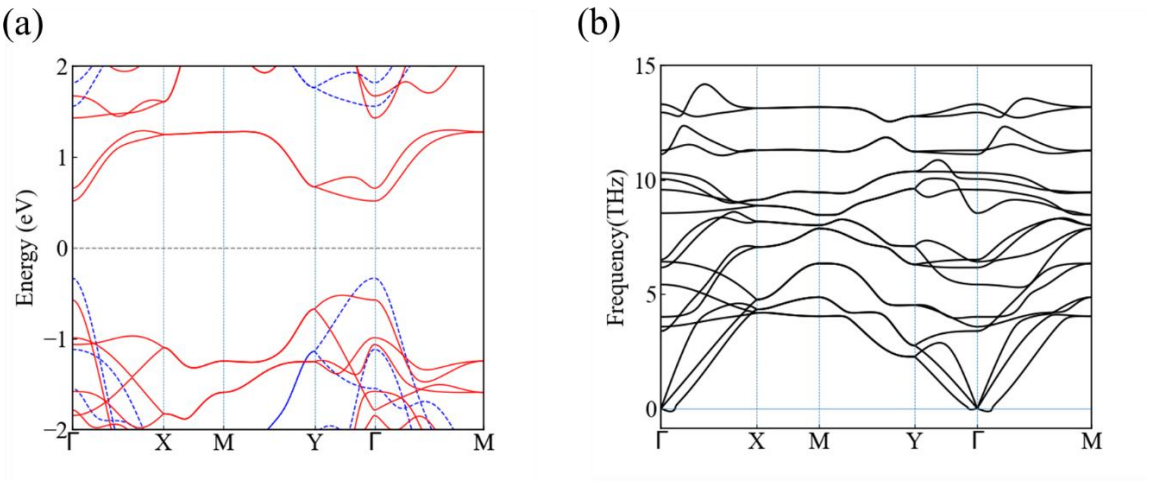

Supplementary Figure 1. (a) Electronic band structure of VSF monolayer where red solid lines and blue dashed lines represent spin-up and spin-down channels, respectively. (b) Phonon spectrum of VSF monolayer.

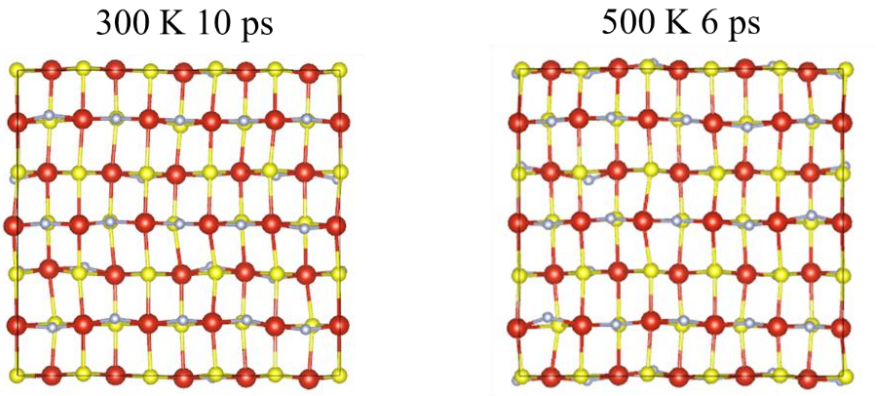

Supplementary Figure 2. Snapshot structures of VSeF monolayer after 10 ps and 6 ps of AIMD simulations at 300 K and 500 K, respectively.

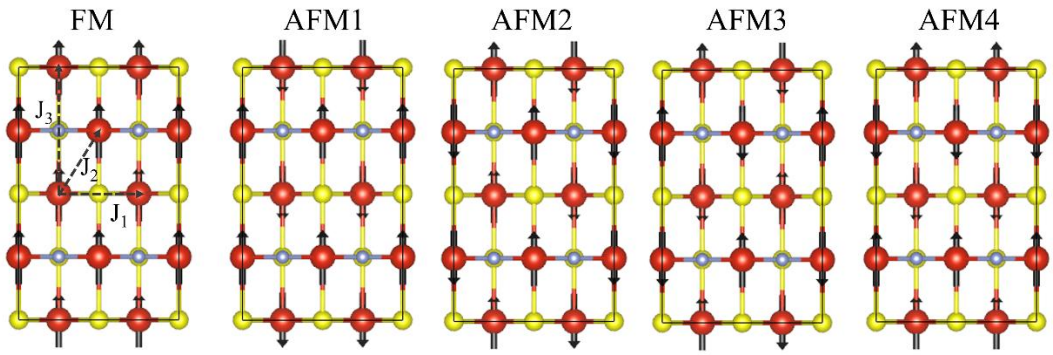

Supplementary Figure 3. Five possible magnetic configurations we considered.

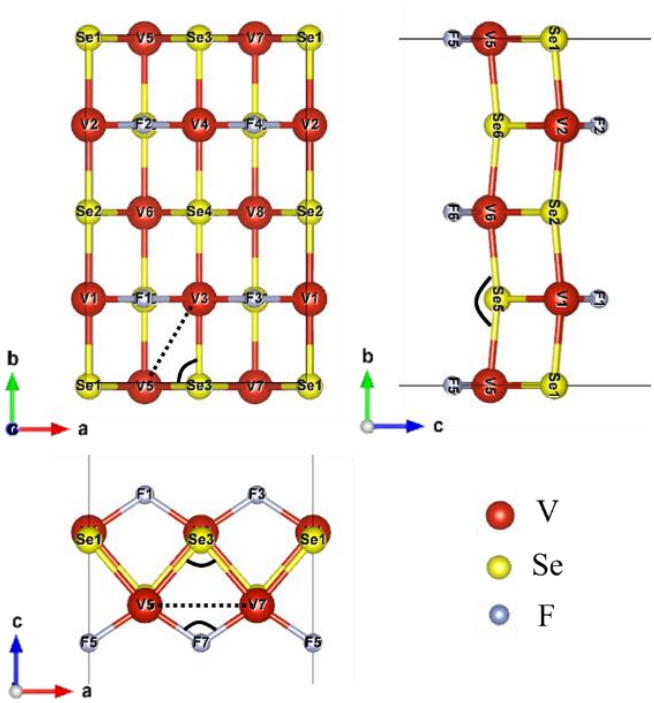

Supplementary Figure 4. Structural details related to the magnetic exchange interaction, such as the distance between magnetic atoms and angels among magnetic atoms and anion ligand.

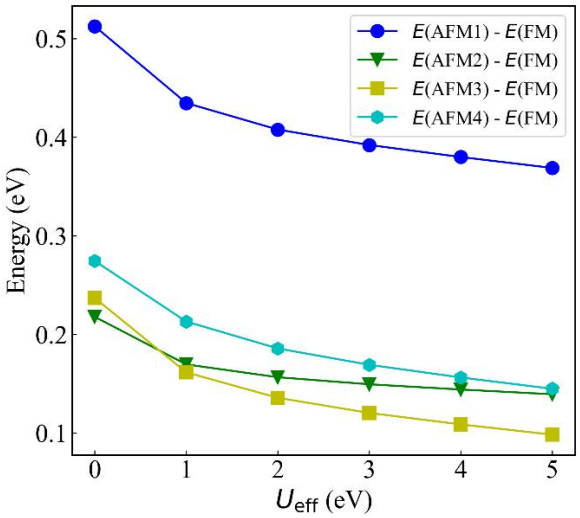

Supplementary Figure 5. Relative energies of 2 × 2 VSeF supercell between five different magnetic configurations as a function of U_{eff}.

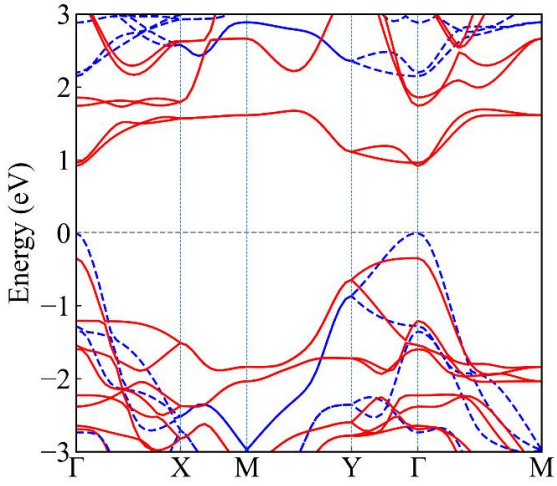

Supplementary Figure 6. Electronic band structure of VSeF calculated with the HSE06 hybrid functional.

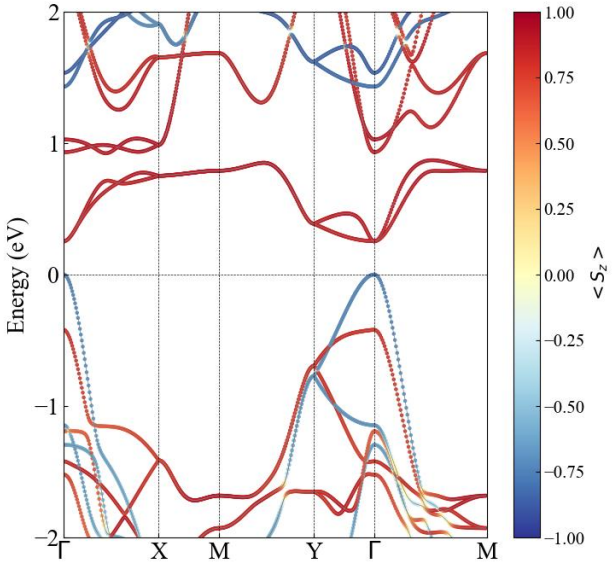

Supplementary Figure 7. Electronic band structure of VSeF monolayer considering SOC effect under [001] magnetization, where the magnitude of spin *z*-component contribution is marked by the color.

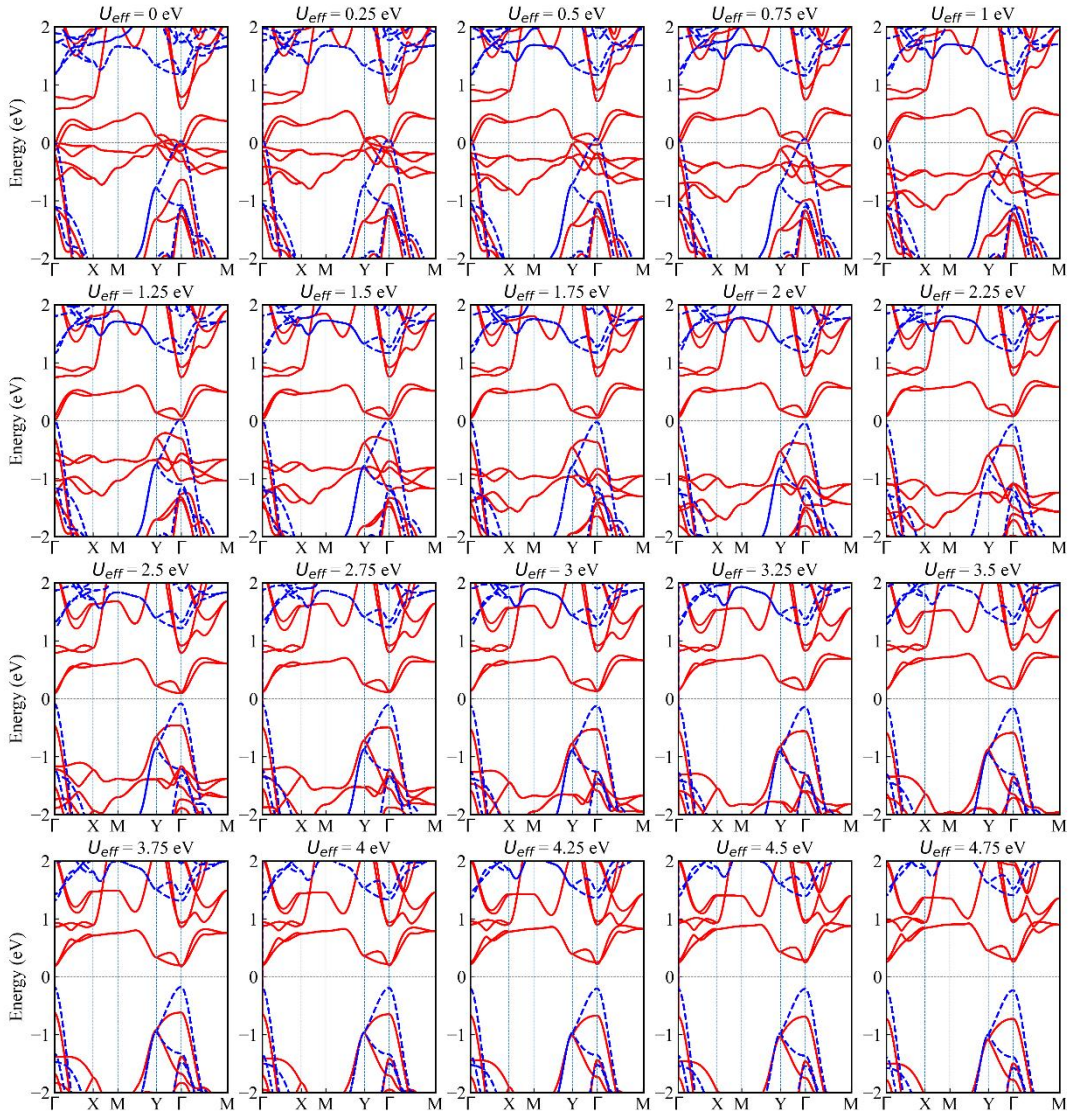

Supplementary Figure 8. Electronic band structures of VSeF calculated with PBE functional under different U_{eff} values.

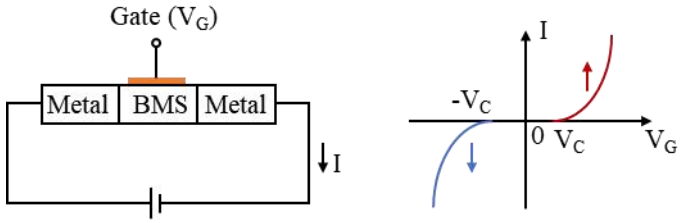

Supplementary Figure 9. Schematic plot of the spin field effect transistor built based on the BMS character. The carriers' spin orientation in the BMS channel can be controlled by the applied gate voltage.

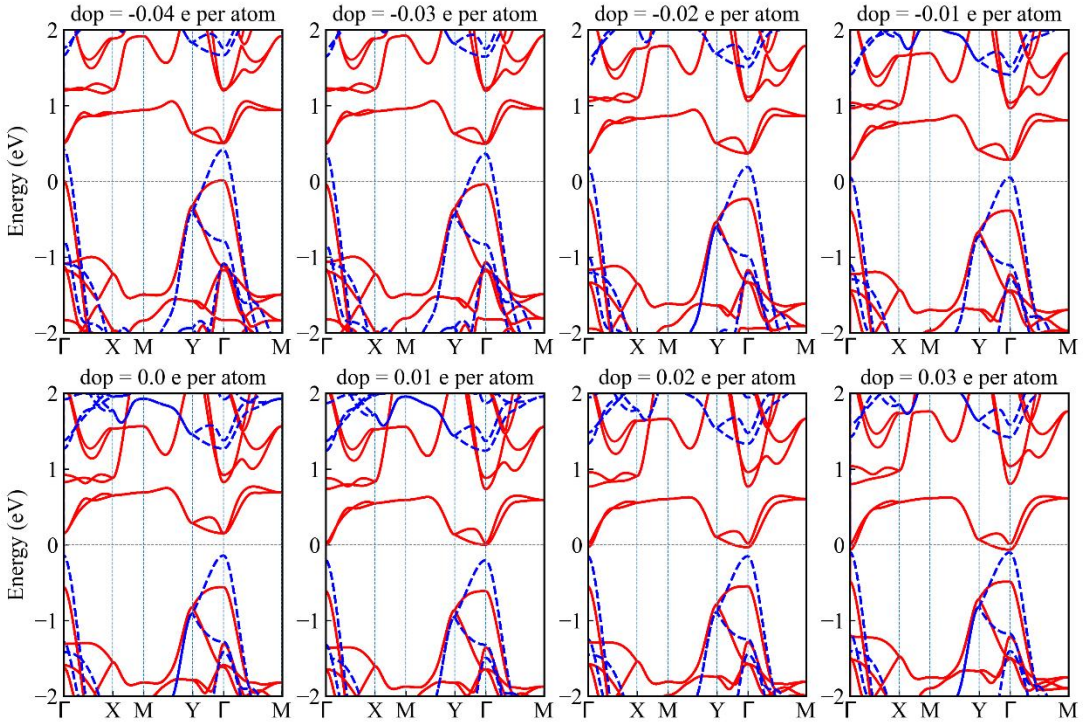

Supplementary Figure 10. Electronic band structures of VSeF under different carrier concentrations. The positive and negative values represent electron doping and hole doping, respectively.

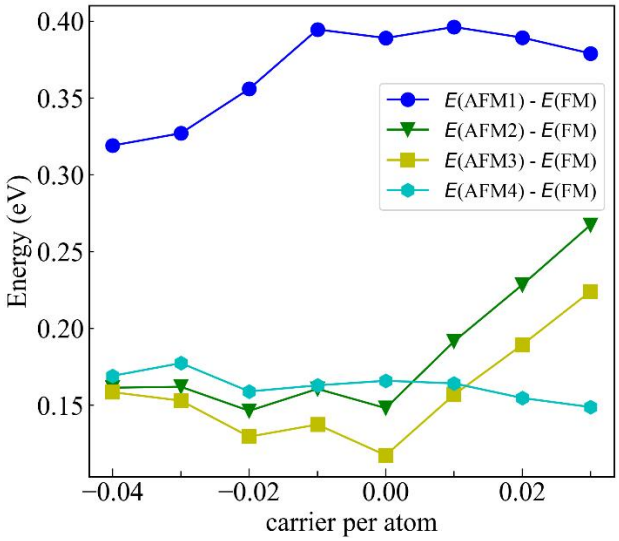

Supplementary Figure 11. Relative energies of 2 × 2 VSeF supercell between five different magnetic configurations as a function of carrier concentration.

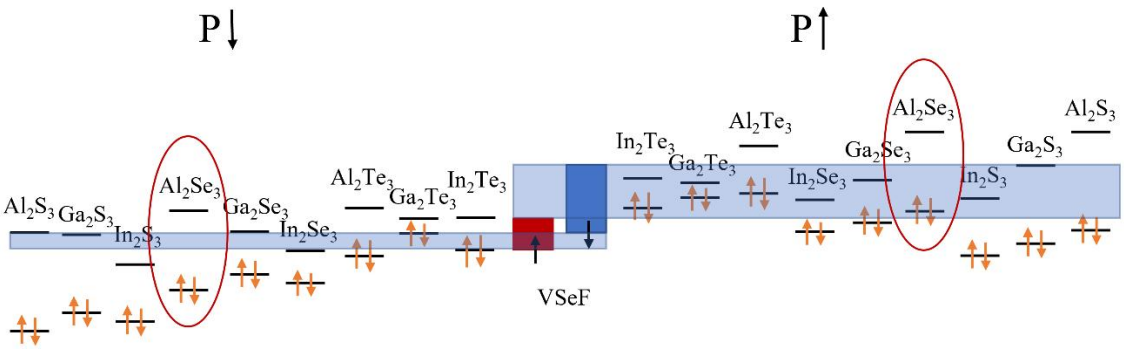

Supplementary Figure 12. Band alignments between VSeF monolayer and 2D III_2-VI_3 ferroelectrics under different ferroelectric polarized states. Due to the limited built-in electric field of monolayer III_2-VI_3 ferroelectrics, it's hard to achieve both *n*-type doping and *p*-type doping in one BMS/FE heterostructure by switching the ferroelectric polarization. Further considering the lattice mismatch, we selected the 2D Al_2Se_3 as the ferroelectric gate.

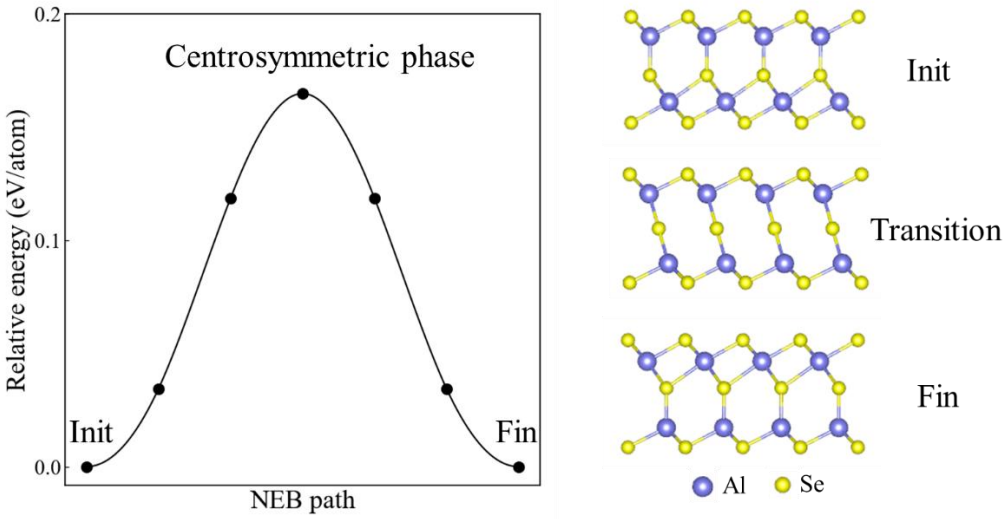

Supplementary Figure 13. Ferroelectric reversal path and barrier of strained Al_2Se_3 monolayer. The initial (Init) and final (Fin) states are ferroelectric polarized states. The transition state is centrosymmetric phase.

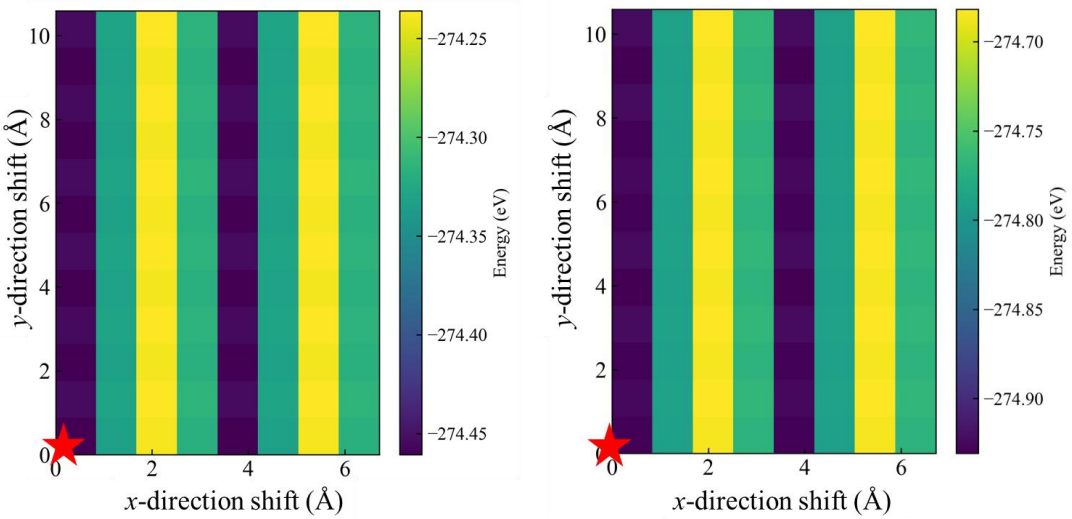

Supplementary Figure 14. The varied total energies of VSeF/Al_2Se_3 bilayer heterostructure as their in-plane relative displacement changes for upward ferroelectric polarization (a) and downward ferroelectric polarization (b). The most stable stacking structures are marked by the red stars.

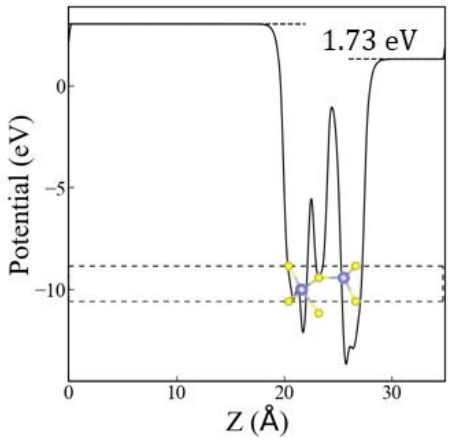

Supplementary Figure 15. *xy*-plane average electrostatic potential of ferroelectric Al_2Se_3 monolayer along the *z* direction.

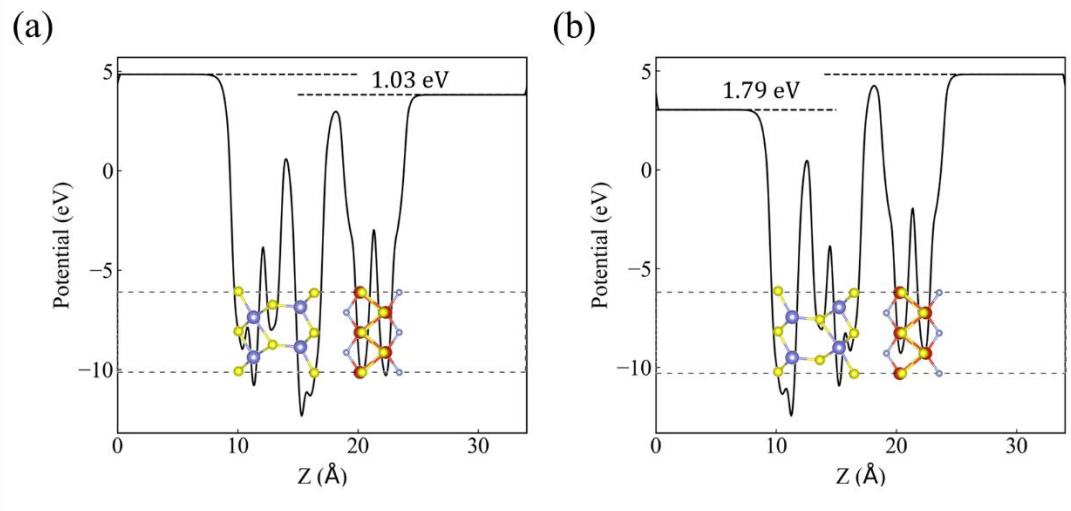

Supplementary Figure 16. *xy*-plane average electrostatic potentials of VSeF/Al_2Se_3 bilayer heterostructure along the *z* direction for upward ferroelectric polarization (a) and downward ferroelectric polarization (b).

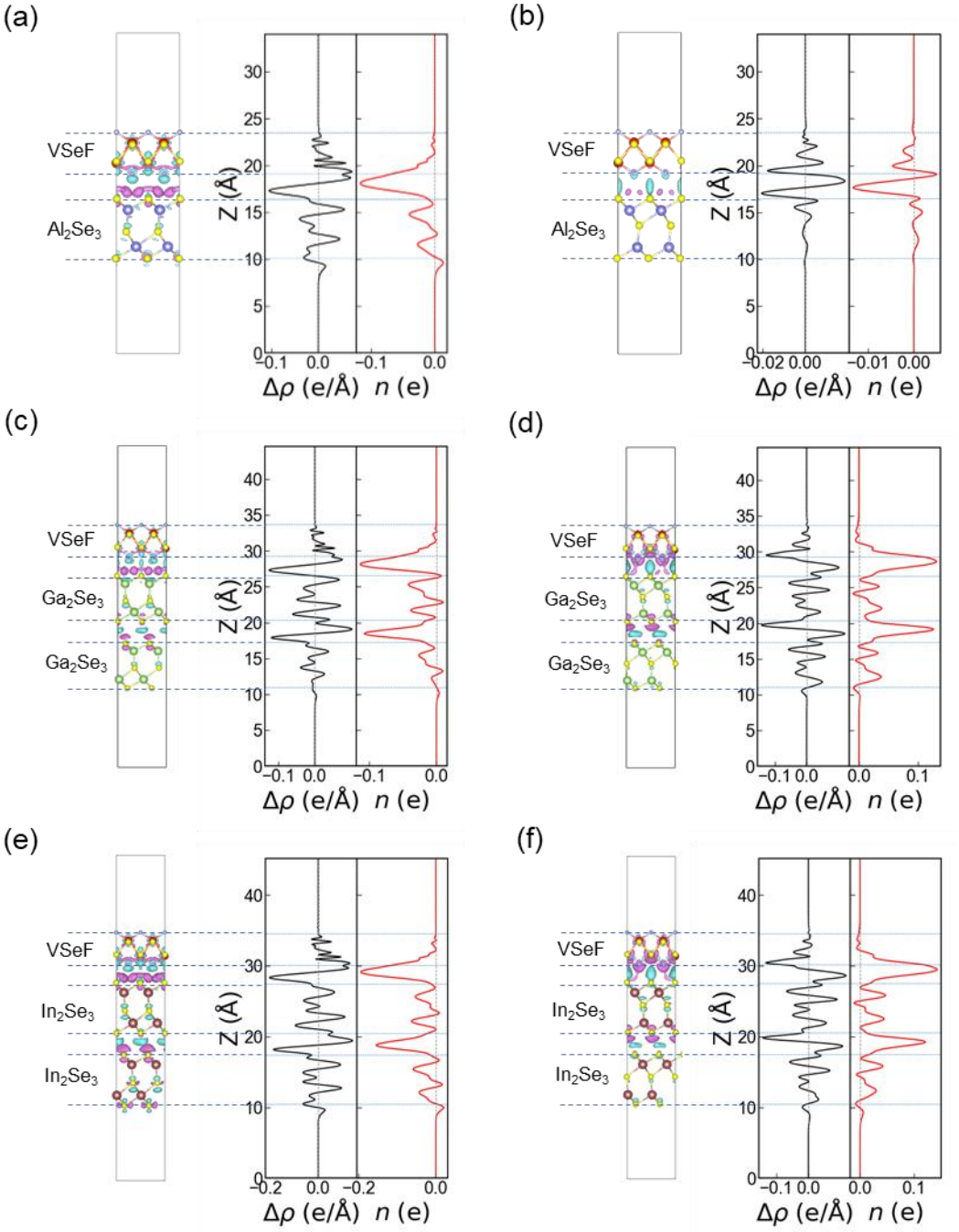

Supplementary Figure 17. Charge density difference, planar-averaged density difference (black line) and the integral (red lines) of planar averaged density difference along *z* direction for VSeF/Al_2Se_3 (↑) (a), VSeF/Al_2Se_3 (↓) (b), VSeF/biGa_2Se_3 (↑) (c), VSeF/biGa_2Se_3 (↓) (d), VSeF/biIn_2Se_3 (↑) (e) and VSeF/biIn_2Se_3 (↓) (f) heterostructures. The blue dashed lines indicate the atomic boundary of each layer, and the cyan and magenta isosurfaces represent electronic accumulation and depletion with isovalue of 2.03×10^{-3} e·Å^{-3}, respectively.

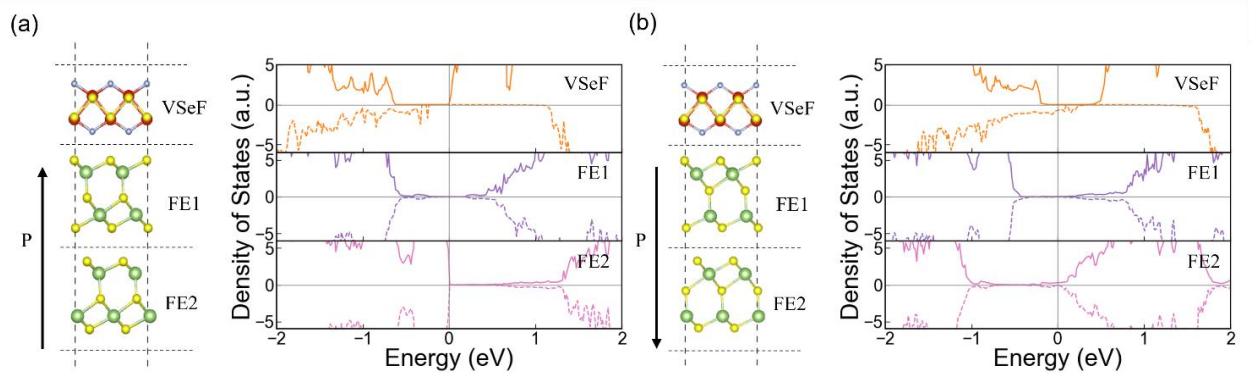

Supplementary Figure 18. Side views of VSeF/biGa_2Se_3 heterostructures and layer-resolved PDOS for upward polarized bilayer Ga_2Se_3 (a) and downward polarized Ga_2Se_3 (b).

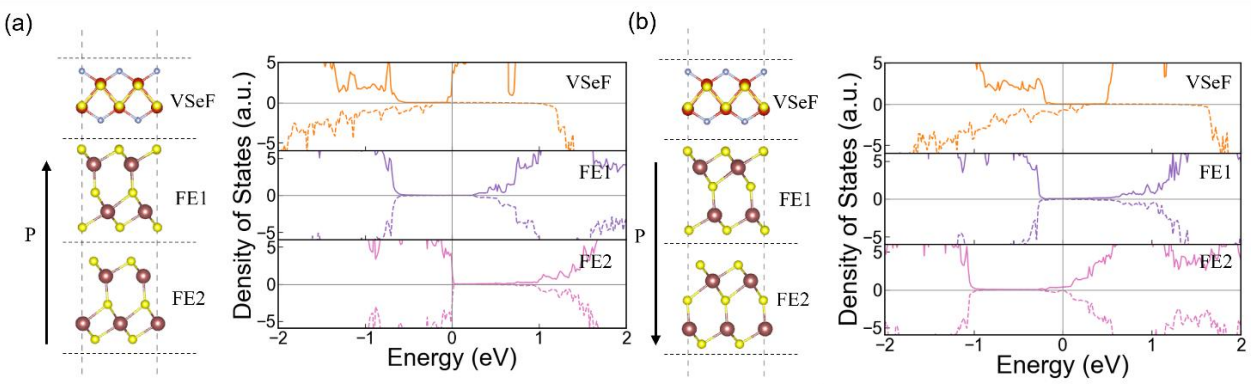

Supplementary Figure 19. Side views of VSeF/biIn_2Se_3 heterostructures and layer-resolved PDOS for upward polarized bilayer In_2Se_3 (a) and downward polarized In_2Se_3 (b).

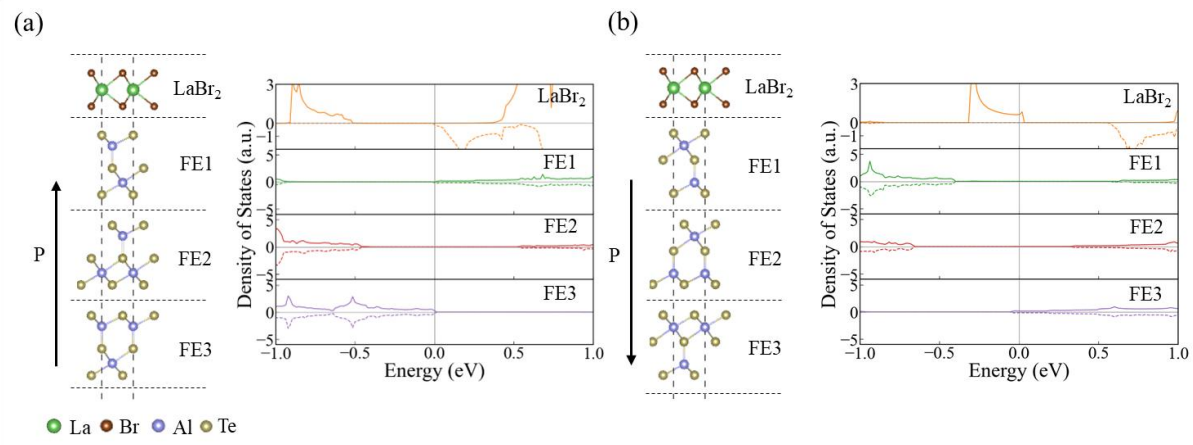

Supplementary Figure 20. Side views of $LaBr_2$/triAl_2Te_3 heterostructures and layer-resolved PDOS for upward polarized Al_2Te_3 (a) and downward polarized Al_2Te_3 (b).

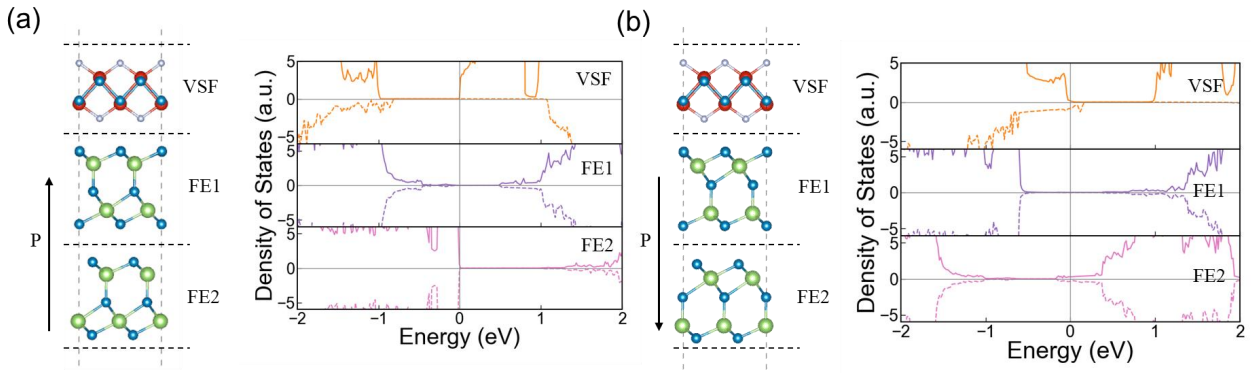

Supplementary Figure 21. Side views of VSF/biGa_2S_3 heterostructures and layer-resolved PDOS for upward polarized Ga_2S_3 (a) and downward polarized Ga_2S_3 (b).